SAR Data for Detecting Landslide Phenomena: The November 26, 2022 Landslide of the Ischia Island (Southern Italy)

Marco Polcari, Emanuele Ferrentino, *Graduate Student Member, IEEE*, Christian Bignami, *Member, IEEE*, Sven Borgstrom, Rosa Nappi, and Valeria Siniscalchi

***Abstract*—In this article, several change detection techniques based on satellite SAR data acquired by Cosmo-SkyMed Second Generation missions have been evaluated aiming at detecting the landslide-mudflow phenomenon triggered by the strong flooding event that hit Ischia Island in November 2022. It severely impacted on Casamicciola Terme area causing damages and collapses of many buildings and unfortunately also casualties. Experimental results show how both single-polarimetric (SP) and dual-polarimetric (DP) techniques are able to detect the main landslide occurring along the northern flank of Mt. Epomeo and in some cases also connected phenomena such as mud accumulation. Additional analyses have been performed to quantitatively evaluate the performance of all of them showing, as in this case, DP techniques outperform the SP ones. The outcomes are then discussed taking into account both the features of each technique and the investigated scenario. Detecting and mapping this kind of phenomenon is important for the evaluation of the affected area, especially for complex scenarios such as Ischia island, and can be very useful to support both the stakeholders for first aid and the civil protection for the post-crisis management.**

***Index Terms*—Change detection, Ischia island, landslide, synthetic aperture radar (SAR) images.**

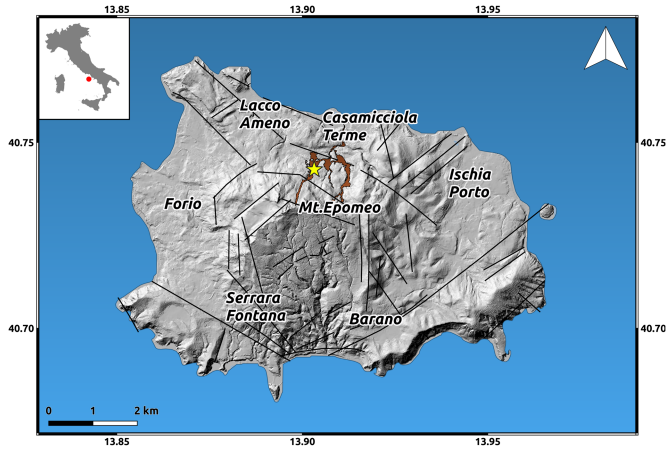

Fig. 1. Focus on Ischia island. Hillshade (2 × 2 m) provided by Nappi et al. [12]. The brown polygon indicates the mapping of the damaged areas (grading product) due to the flooding, retrieved by the Copernicus Emergency Management Service (https://emergency.copernicus.eu/). The yellow star represents the epicenter of the earthquake occurred on August 21st, 2017 from INGV source (Osservatorio Nazionale Terremoti). The black lines are the faults from [13].

I. Introduction

ON NOVEMBER 26th, strong flooding hit Ischia island, in the Gulf of Naples (southern Italy), causing several problems to the infrastructures and triggering a landslide characterized by huge mudflow on Mt. Epomeo, in the hamlet of Casamicciola Terme (see Fig. 1). Unfortunately, the mudflow violently hit the urban area of Casamicciola Terme, completely destroying some buildings, severely damaging and submerging more than thirty private residences, and dragging several cars into the sea. The search for the missing by the Italian Civil Protection, the Fire Brigade, and volunteers lasted several days, making it even more difficult due to adverse weather conditions and unfortunately, in the end, there were 12 casualties. The Italian government promptly declared a state of emergency and allocated 4 million euros to provide immediate relief to the local population affected by the landslide-mudflow with more than 200 residents left homeless. It is not the first time that Ischia has been at the center of media attention, being it an island of volcanic origin characterized by ground deformation and seismic activity which are constantly monitored by seismic and geodetic ground-based networks of the Istituto Nazionale di Geofisica e Vulcanologia (INGV) [1], [2], [3] and through remote sensing data [4]. In August 2017, many damages and collapses were registered in Casamicciola following a shallow M_w 3.9 earthquake, which also triggered another huge landslide on the same flank of Mt. Epomeo [5], [6], [7]. Now, the landslide-mudflow interested a more localized sector of Mt. Epomeo, indeed it was channeled into a narrow drain, likely formed due to the morphology and previous water erosion phenomena, before reaching the urban area of Casamicciola via a road called

Manuscript received 1 March 2023; revised 24 April 2023 and 24 May 2023; accepted 8 June 2023. Date of publication 16 June 2023; date of current version 3 July 2023. *(Corresponding author: Marco Polcari.)*

Marco Polcari, Emanuele Ferrentino, and Christian Bignami are with the Osservatorio Nazionale Terremoti Section, Istituto Nazionale di Geofisica e Vulcanologia, 00143 Rome, Italy (e-mail: marco.polcari@ingv.it; emanuele.ferrentino@ingv.it; christian.bignami@ingv.it).

Sven Borgstrom, Rosa Nappi, and Valeria Siniscalchi are with the Osservatorio Vesuviano Section, Istituto Nazionale di Geofisica e Vulcanologia, 80125 Naples, Italy (e-mail: sven.borgstrom@ingv.it; rosa.nappi@ingv.it; valeria.siniscalchi@ingv.it).

Digital Object Identifier 10.1109/JSTARS.2023.3286993

Via Celario. Mapping the path of the landslide-mudflow is not straightforward but of primary importance to better understand the dynamic and the causes of the phenomenon and to prevent future natural disasters. This is generally performed by visual inspection of optical satellite imagery although they are acquired only with sunlight and can be largely affected by cloud coverage [8], [9]. In this context, satellite data acquired from synthetic aperture radar (SAR) microwave sensors can provide a useful instrument offering a synoptic view of the observed areas sunlight independently, in any atmospheric conditions, and with a temporal sampling of a few days. Several works on the use of SAR data for landslides detection were already performed; however, they focused on the detection of huge single events or the classification of large areas interested in landslide phenomena [10], [11]. Instead, the Ischia case study is quite challenging since the natural channel where the landslide-mudflow triggers is narrow (a few meters) and hard to be detected considering the resolution of the SAR sensors. Moreover, the investigated scenario is very complex being characterized by rough topography, vegetation, mud, and urban areas. Then, in this work, several SAR-based techniques applied to *X*-band Cosmo-SkyMed Second Generation (CSG) images have been investigated to explore the capability of the satellite radar signal to map and detect such kinds of phenomena. Depending on the revisit time of the acquisitions, such kind of information can be exploited for rapid mapping and hazard assessment purposes thus supporting the stakeholders in the rescue of missing and in the management of postcrisis scenarios.

II. Geological Settings

Ischia is an active volcanic island located in the Gulf of Naples (Southern Italy) belonging to the Phlegraean Volcanic District, which also includes the Campi Flegrei caldera, Procida, and Vivara islands. The Ischia island represents the subaerial portion of a volcanic complex characterized by a long eruptive history since at least 150 thousand years Before Present (ka B.P.) [14]. The main activity has been the Green Tuff eruption (55 ka B.P.) with the consequent collapse of the caldera in the central sector of the island. After this event, a large resurgence process resulted in the emplacement of the Mt. Epomeo block starting from 30 ka B.P. [15], with the maximum uplift in the order of about 900 m. The resurgent block is bordered by a normal faults' system producing a morphologically well-defined Holocene graben structure at the base of the northern flank of Mt. Epomeo [16]. Despite this large resurgence interesting the central part of the island, the south-central part is characterized by general subsidence pointed out by geodetic data [17], [18]. The last period of the volcanic activity started 10 ka B.P. with 46 different eruptions mainly between 2900 years B.P. and 1302 A.D. (the Arso eruption). As a consequence, Mt. Epomeo's flanks are characterized by slope instability at different scales from shallow mass movements to large rock and debris avalanches. These phenomena typically occurred during eruptions, earthquakes (e.g., during the last seismic sequence at the end of August 2017), or extreme meteorological events as it happened on November 26th, 2022 [4], [5], [6], [7], [19], [20].

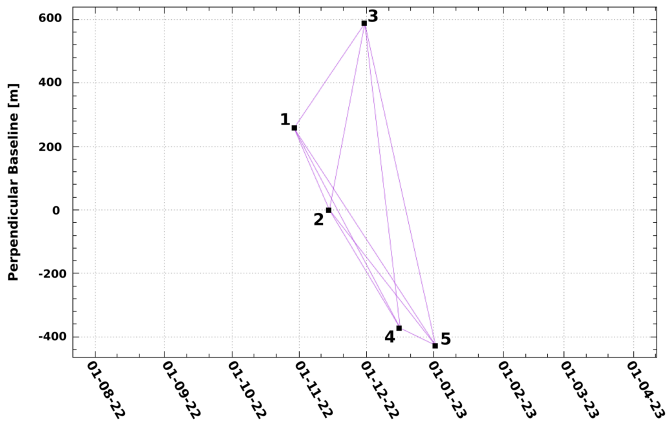

Fig. 2. Perpendicular/temporal baseline chart between all the pairs.

III. SAR Data

Because of the small size of the phenomenon to be investigated, the high-resolution *X*-band SAR data are the most suitable to be applied in the present study. Therefore, the acquisitions from CSG mission were exploited since they offer a pixel ground resolution of about 2 × 2 m, which is one of the best in the framework of free accessible non-commercial products. The exploited dataset consists of five dual-polarimetric (DP) (HH+HV) Single Look Complex (SLC) images acquired in strip map mode between October 30th, 2022 and January 1st, 2023 along the descending track and with a revisit time of 16 days. The geometry of acquisition of all the images is characterized by an incidence angle of about 27° and an azimuth angle of about 11°. To reduce the speckle noise characterizing the SLC SAR images, despeckling filtering [21], [22] using a window of 9 × 9 pixels along both range and azimuth was preliminary applied. In Fig. 2, the chart of both perpendicular and temporal baselines between all the pairs is shown. According to the scheduling of the CSG mission, there is an acquisition every 16 days, whereas the orbital tube of the mission is not so narrow with values of perpendicular baseline up to 1000 m. For geocoding the output products, the Digital Elevation Model (DEM) by Nappi et al. [12] was used. It has been obtained by digitizing contour maps and spot elevation in vector format (scale 1:2000) provided by the Consorzio Intercomunale Servizi Ischia. In particular, the triangulation irregular network interpolation technique through ArcGIS ESRI Software was used. Vector data of the coastal line were derived from both the digital color orthophoto (pixel 1 m) of Compagnia Generale Riprese Aeree, airborne 2000, and an IKONOS satellite image (RGB, pixel 1 m) acquired on August 9th, 2000. This process produced a 2 × 2 m DEM with an elevation range spanning 0–787.4 m. The DEM is referenced to UTM zone 33 with the WGS-84 ellipsoid.

IV. Detection Methods

In this section, the theoretical rationale that underpins the proposed multipolarization methodologies aiming at imaging any changes due to the landslide is described.

A. Coherence Variation

The coherence maps between two SAR images indicate the correlation degree of the images. They can be estimated, pixel by pixel, according to the following equation:

$$\gamma_{\text{pre/post}} = \frac{\langle x_1(k)\, x_2^*(k)\rangle}{\sqrt{x_1(k)\, x_1^*(k)\cdot\langle x_2(k)\, x_2^*(k)\rangle}} \tag{1}$$

where $x_1(k)$ and $x_2(k)$are the complex values of the pixel k for the first and the second images, x^* is the complex conjugate of x, and $< >$ is the averaging module. The coherence is a parameter sensitive to any changes occurring in the investigated area along the time interval between the acquisitions, impacting both the phase and the amplitude of the SAR signal. It is a normalized metric with values spanning between 0 and 1. High values of the coherence represent quite unchanged scenarios according to the incidence SAR signals, indeed they are typically found in urban areas. Conversely, lower values are typically related to scenarios that change very quickly in time producing temporal decorrelation effects such as sea or vegetated areas. Then, modifications of the observed scenarios due to natural or anthropogenic phenomena such as the landslides-mudflow that hit Ischia island should theoretically modify the electromagnetic response of the soil producing some changes in the coherence values. Depending on the features of the investigated scenario, the detection methods based on the coherence are usually performed by using three SAR images: 1) two images pre-event and one image postevent to evaluate the coherence loss during an event [23], [24] or 2) one image pre-event and two images postevent to evaluate any coherence increase after the event [10]. Here, the second approach was conceptually followed by using four SAR images, a pair before and a pair after the event. Indeed, the co-event pair was discarded due to the large perpendicular baseline of about 600 m, which could affect the results. Then, the coherence pre- and post-event were estimated and any variations of such parameters can be highlighted by considering the difference of the two:

$$\Delta\gamma = \gamma_{\text{post}} - \gamma_{\text{pre}}. \tag{2}$$

B. Differences in the Radar Backscattering

An electromagnetic wave that travels through time and space can interact with a specific target. During this interaction, some of the energy carried by the incident wave (E_I) is absorbed by the target while the remaining energy is emitted as a scattered electromagnetic wave (E_S) [25].

One way to quantify this interaction is using the normalized radar cross section (NRCS), which measures the amount of electromagnetic energy scattered back to the radar by the target. The NRCS depends on several factors including the wave frequency and polarization. Hence, to take into account polarization effects, if we denote by p the polarization of the incident field (E_I) and by q the polarization of the scattered field (E_S), the polarization-dependent NRCS can be defined as follows [25]:

$$\sigma^0_{qp} = \frac{(4\pi d^2)}{A_0}\frac{\left\langle |\boldsymbol{E}_{Sq}|^2\right\rangle}{\left\langle |\boldsymbol{E}_{Ip}|^2\right\rangle} \tag{3}$$

where $\{p, q\} \in \{\text{H}, \text{V}\}$ when a linear horizontal (H)–vertical (V) orthogonal basis is adopted, d represents the distance between the SAR and the target, A_0 is the illuminated area, and $|\cdot|$ is the modulus operator.

NRCS, also called the backscattering coefficient, is highly sensitive to the type of target included in the observed scene [25]. This means that different targets or targets modified over time due to natural or anthropogenic effects give different backscattering values. Following this rationale, the change detection approach aiming at evaluating any changes over the observed scene due to the landslide-mudflow affecting Ischia island is based on the differences in the polarized backscattering intensity

$$\Delta I = \frac{I_{\text{post}} - I_{\text{pre}}}{I_{\text{post}} + I_{\text{pre}}} \tag{4}$$

where the subscripts pre and post are related to imagery collected before and after the event, respectively, and I stands for the NRCS evaluated for the copolarized (HH) and cross-polarized (HV) channel

$$I_{\text{HH}} = \sigma^0_{\text{HH}} \tag{5}$$

$$I_{\text{HV}} = \sigma^0_{\text{HV}}. \tag{6}$$

Note that, (4) is normalized with the sum of the features evaluated before and after the event.

C. Difference of Covariance Matrices

The observation of changes induced by natural or anthropogenic phenomena including landslides and flooding can be also performed using a DP scattering-based change detection approach proposed in [26] and [27]. In such case, a covariance change detection matrix based on the difference between two covariance matrices collected before and after the event is constructed [26]

$$C_{\text{CD}} = \frac{C_2 - C_1}{C_2 + C_1} \tag{7}$$

where C_1 and C_2 are the covariance matrices that refer to DP SAR scenes collected before and after the event, respectively. To find the scattering mechanisms $\underline{\omega}$ that maximize the changes from the pre-to the post-event imagery, a Lagrange optimization procedure is undertaken that results in the following eigenvalue problem [28]:

$$C_{CD}\underline{\omega} = \lambda_j\underline{\omega} \tag{8}$$

where λ_j (with $j = 1, 2$) are the eigenvalues that maximize/minimize the difference between two covariance matrices. The largest eigenvalue λ_1 of the matrix C_{CD} is mainly positive, which means that it represents the power of scattering contributions that increase or appear in the scene observed in the post-event, whereas the smallest eigenvalue λ_2 is mostly negative, which means that it represents the power of scattering

mechanisms that are reduced or disappear in the scene observed in the post-event [26]. A complex event, such as a landslide, together with the geometry of acquisition of the SAR, needs complementary information given by both $\lambda_1$and λ_2 to better detect the fracture shape due to the landslide.

Hence, to take into account every possible change, the two eigenvalues are properly combined by arithmetic mean given by [26]

$$\lambda = \frac{\lambda_1 + \lambda_2}{2}. \tag{9}$$

D. Reflection Symmetry

The second DP change detection approach exploits the property of reflection symmetry [29], and it is based on the amplitude of the interchannel correlation given by

$$r = \left|\langle S_{xx} S_{xy}^{*} \rangle\right| \tag{10}$$

where S_{xx} and S_{xy} are the co-polarized and cross-polarized scattering elements, respectively.

This property is verified when dealing with naturally distributed scenes, such as vegetated areas. In fact, over this kind of scenario, a very low correlation between co-polarized and cross-polarized channels is expected, i.e., r about 0 [30]. On the other hand, when a phenomenon like a landslide is observed, it is expected that it breaks the natural scenario and, as a consequence, reflection symmetry no longer applies. This implies that non negligible r values are expected [30]. For the purpose of this study, r is expected to be close to zero when dealing with a natural scenario, whereas significant departures from this reference condition are expected over areas where landslides occurred. Hence, to detect the area affected by the landslide-mudflow, the following change detection feature is considered [31]:

$$\Delta r = \frac{r_{\text{post}} - r_{\text{pre}}}{r_{\text{post}} + r_{\text{pre}}} \tag{11}$$

where r_{pre} and r_{post} are the reflection symmetry maps evaluated before and after the event. This suggests large (low) Δr values over areas affected (not affected) by natural or anthropogenic phenomena.

V. Results

A. Multilooked Intensity (MLI) Images

A first prompt analysis consists of a simple visual comparison between the multilooked intensity (MLI) of the images acquired just before and after the event. Then, in this case, the CSG SAR images acquired on November 15th and December 1st, 2022 were considered. Indeed, any changes in the investigated area affect the backscattering coefficient thus producing different intensity signals. Such visual comparison is shown at the scale of Ischia island (see Fig. 3) and in a region of interest (ROI) focusing on the area affected by the event (see Fig. 4). Different intensity values are observed along the flank of Mt. Epomeo interested by the landslide-mudflow. In particular, a section of the path followed by the phenomenon, also evidenced by Copernicus Emergency Management Service

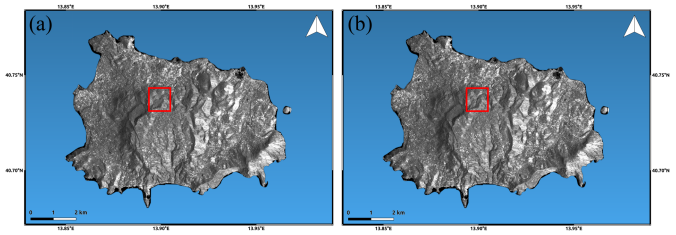

Fig. 3. Comparison between the intensity of multilooked CSG images acquired on November 15th [A] and December 1st [B], 2022. The red rectangle indicates the area of interest (AOI) affected by the landslide.

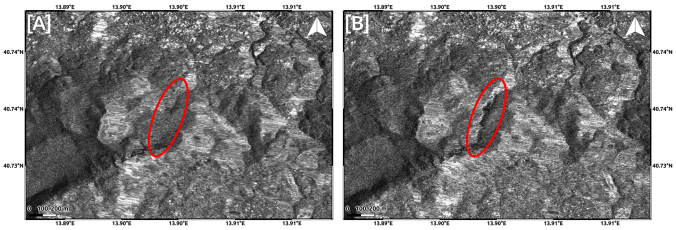

Fig. 4. Focus on the AOI shown in Fig. 3: comparison between the intensity of multilooked CSG images acquired on November 15th [A] and December 1st [B], 2022. The landslide activated by the flooding is indicated by the red ellipse and clearly visible in the postevent image (panel B).

(https://emergency.copernicus.eu/), is quite clear and it is highlighted by the red ellipse in Fig. 4.

B. Coherence Variation

Any changes in the area affected by the event, due to the landslide, the mud covering the urban area of Casamicciola, and to some buildings collapse, should produce a coherence variation. Then, to perform such analysis, two pairs of CSG SAR images, acquired before and after the flooding event of the 26th, were exploited considering the difference of the coherence post- and pre-event.

In particular, the two pairs considered for the coherence analysis consist of the images acquired on October 30th and November 15th, 2022 for the pre-event and on December 17th, 2022 and on January 2nd, 2023 for the post-event. Indeed, the same temporal baseline of 16 days between images should guarantee the same effects of temporal decorrelation for the two pairs. Instead, the pair co-event, i.e., the one formed by the images acquired on November 15th and December 1st, and the pair just following the event, i.e., the one formed by the images acquired on December 1st and 17th, were discarded due to the huge perpendicular baseline value of about 600 and 1000 m, which could introduce some geometric decorrelation effects thus affecting the results. The result of such analysis is shown in Fig. 5. As can be noticed, there is an increase in the post-event coherence which seems to define quite well the path of the landslide-mudflow along the flank of Mt. Epomeo. Moreover, some localized patterns of increased coherence are also observed in the surroundings, especially considering the urban area of Casamicciola located in the northern part of Mt. Epomeo.

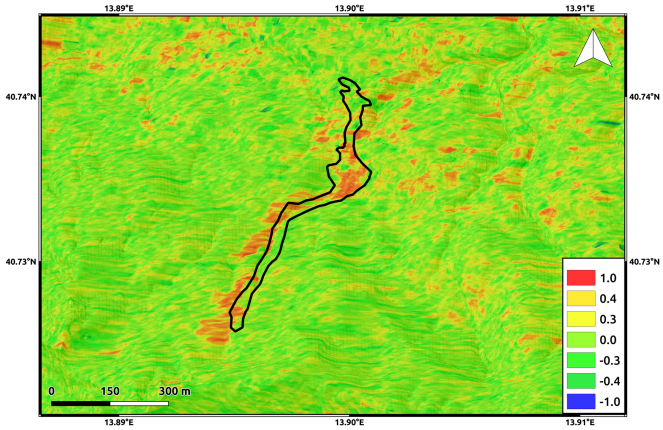

Fig. 5. Map of difference of coherence between post and pre-event image pairs. The black polygon indicates the mapping of the impact and spatial extent of the landslide-mudflow retrieved by the Copernicus Emergency Management Service (https://emergency.copernicus.eu/).

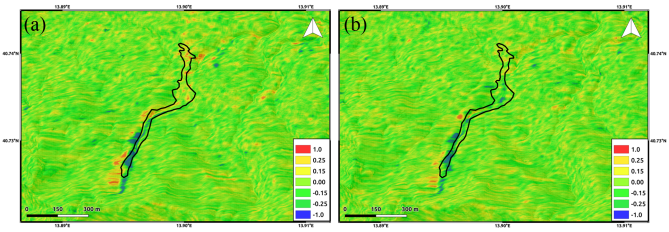

Fig. 6. Maps of NRCS difference between post- and pre-event images (change detection) estimated with (a) HH and (b) HV channels. The black polygon indicates the mapping of impact and spatial extent of the landslide-mudflow (delineation product) retrieved by the Copernicus Emergency Management Service (https://emergency.copernicus.eu/).

C. Normalized Radar Cross Section (NRCS)

The backscattering analysis has been performed with the CSG images acquired on November 15th and December 1st using both the co-polarized (HH) and cross-polarized (HV) channels. The metric ΔI is depicted in Fig. 6(a) and (b) for the HH and HV channels, respectively. By visually inspecting, it can be noted that both channels detect the changes associated with the landslide-mudflow. Although the results are pretty similar to each other, little differences between co-polarized and cross-polarized channels are visible. The pattern is well emphasized with respect to the surroundings and it is represented as a red and a blue stripe for positive and negative values, respectively. The red stripe is related to an increase in the backscattering signal, whereas the blue stripe represents backscattering values lower in the post-event image than in the pre-event one. Such behavior is also consistent with both the reference black polygon and the MLI images shown in Figs. 3 and 4 where, from west to east, two stripes of increased and decreased intensity values are detected in the image acquired on December 1st, 2022.

D. Differences of Covariance Matrices

The first DP analysis has been performed with the CSG images acquired on November 15th and December 1st. The λ image

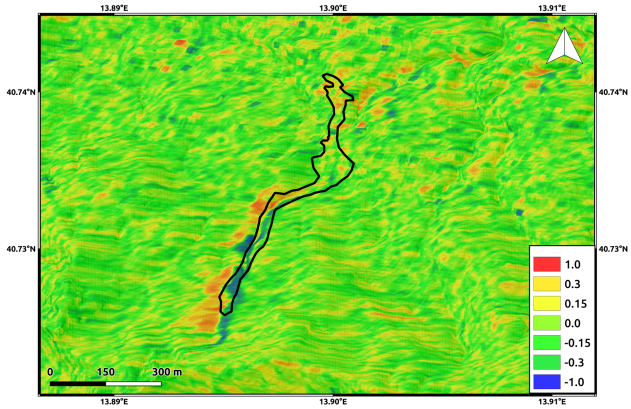

Fig. 7. False-color λ imagery obtained from the CSG dataset collected on November 15th and December 1st. The black polygon indicates the mapping of impact and spatial extent of the landslide-mudflow (delineation product) retrieved by the Copernicus Emergency Management Service (https://emergency.copernicus.eu/).

(9) is depicted in false color in Fig. 7, where the area affected by the landslide-mudflow is enclosed in the black polygon. By visually inspecting, it is possible to observe how the pattern is well emphasized with respect to the surroundings and it quite well matches the reference black polygon. The detected pattern is represented as a red stripe and a blue stripe for positive and negative values, respectively. The red (blue) stripe is related to an increase (decrease) in the power of the scattering mechanisms over the post-event observation. Even in this case, such behavior is also consistent with the MLI images shown in Figs. 3 and 4 where, from west to east, two stripes of increased and decreased intensity values are detected in the image acquired on December 1st, 2022.

E. Reflection Symmetry

The second DP analysis has been performed with the CSG images acquired on November 15th and December 1st. The change detection method Δr (11) is shown in Fig. 8 where the area affected by the landslide-mudflow is enclosed in the black polygon. By visually inspecting, it can be noted that the pattern is well distinguished from the surroundings, and it quite well matches the reference black polygon. The detected pattern is represented as red (negative value) and blue (positive value) stripes, which correspond to an increase and decrease of the symmetry over the post-event observation, respectively. This result can be explained by the fact that the landslide-mudflow occurred over a natural scenario where the reflection symmetry property is satisfied (values of $\Delta r \approx 0$). Hence, under this condition, such a phenomenon breaks the symmetry of the scene resulting in Δr values far from 0.

Once again, according to the previous analysis, such behavior is also consistent with the MLI images shown in Figs. 3 and 4 where, from west to east, two stripes of increased and decreased intensity values are detected in the image acquired on December 1st, 2022.

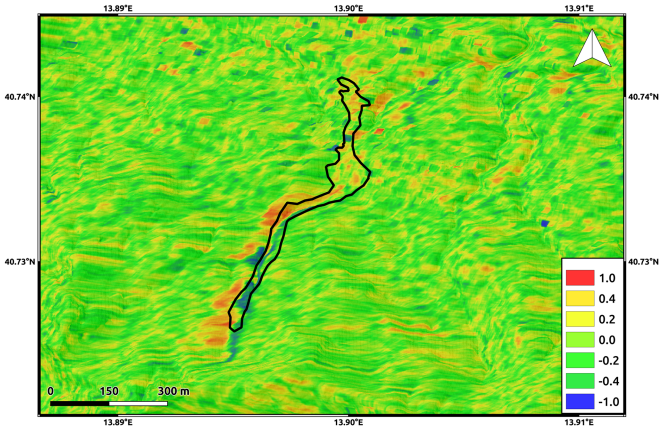

Fig. 8. False-color Δr imagery obtained from the CSG dataset collected on November 15th and December 1st. The black polygon indicates the mapping of impact and spatial extent of the landslide-mudflow (delineation product) retrieved by the Copernicus Emergency Management Service (https://emergency.copernicus.eu/).

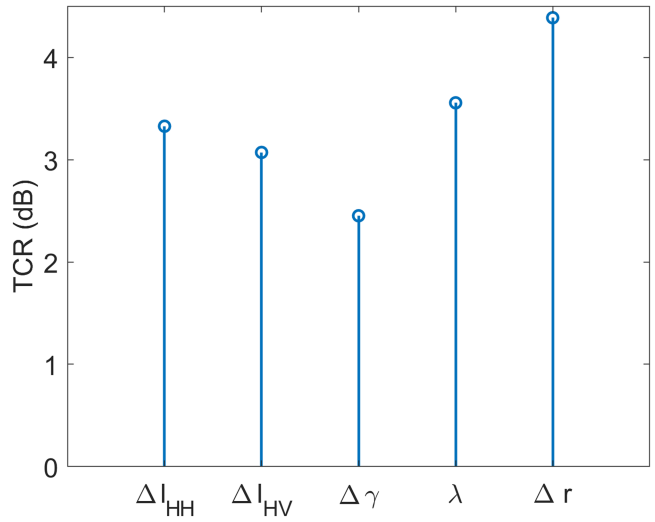

Fig. 9. TCR of each detection method.

F. Quantitative Analysis

To evaluate the performance of multi-polarimetric features in landslide-mudflow detection, a target-to-clutter ratio (TCR) analysis is addressed, which is defined as follows [32]:

$$\mathrm{TCR} = 10 \cdot \log_{10}\left(\left|\frac{X_t}{X_c}\right|\right) \tag{12}$$

where $X \in \{\Delta I_{\mathrm{HH}}, \Delta I_{\mathrm{HV}}, \Delta\gamma, \lambda, \Delta r\}$ is the mean value of the feature evaluated within the ROI excerpted over the landslide (subscript t) and the surrounding environment (subscript c).

Results, depicted in Fig. 9, show that the DP features, i.e., λ and Δr, outperform the single-polarimetric (SP) ones in terms of landslide/surrounding environment separability, with TCR values up to 4.5 dB. In particular, the reflection symmetry technique based on the change detection feature Δr shows the best performance with a separability around 1 dB more than the best SP ones represented by ΔI_{HH}. The worst performance is shown by the coherence-based technique, $\Delta\gamma$, with a TCR value around 2 dB less than Δr. It can be also noted that the copolarized feature (ΔI_{HH}) slightly outperforms the cross-polarized one (ΔI_{HV}).

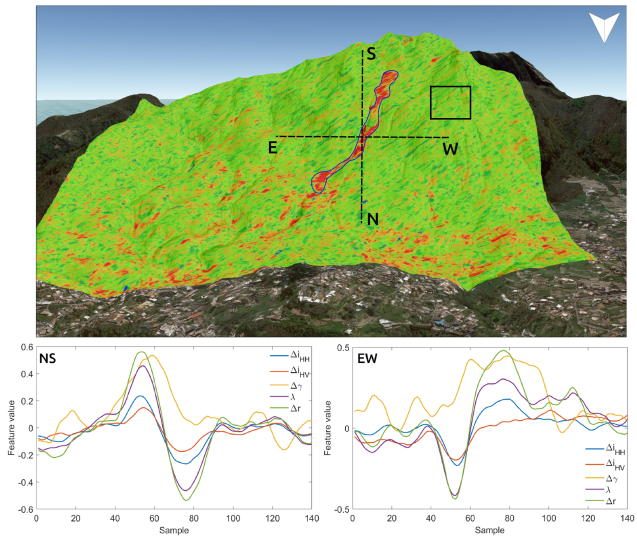

Fig. 10. Trend of all the detection methods along the two transects shown in the figure upward crossing the landslide from North to South [NS] and East to West [EW]. Blue and black polygons indicate the areas used for the estimation of target and clutter, respectively.

To deeper analyze the performance of the detection methods, their behavior is evaluated along the two transects shown in Fig. 10 crossing approximately from north to south (NS) and from east to west (EW) the landslide/surrounding environment boundary.

Both the NS and the EW transects show how $\Delta I_{\mathrm{HH}}, \Delta I_{\mathrm{HV}}$, λ, and Δr are characterized by two peaks with respect to the background corresponding to the two stripes of increased and decreased values related to the landslide. In addition, these techniques show the same trend along both transects with similar values of bandwidth of the two peaks representing the landslide-mudflow. However, in terms of amplitude, the DP techniques, Δr and λ, outperform up to about 50% of the SP ones with the best performances shown once again by Δr. On the other hand, $\Delta\gamma$ shows only one peak corresponding to the stripe of increased coherence after the event. The amplitude is comparable with the one of Δr but it is characterized by a greater bandwidth especially considering the EW transect where it is about twice that of the other techniques. This means that a larger number of pixels are sensitive to variations of coherence instead of the other parameters.

VI. Discussion

SAR-based techniques adopted in the present work show their capabilities in detecting the landslide-mudflow causing several damages on Ischia island. All the retrieved outcomes are consistent with the rapid mapping analysis performed by the Copernicus Emergency group.

The pattern retrieved by $\Delta i_{\mathrm{HH}}, \Delta i_{\mathrm{HV}}, \lambda,$ and Δr analysis is quite similar. They all are able to detect the upper part of the phenomenon along the flank of Mt. Epomeo showing, from East to West, two stripes of increased and reduced values of intensity

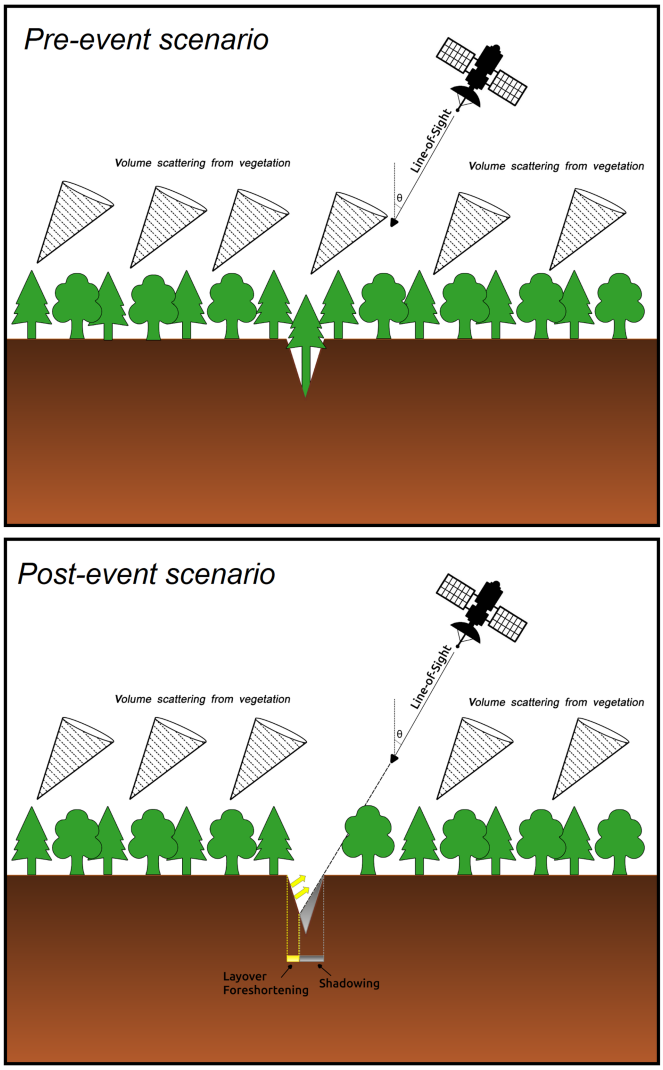

Fig. 11. Investigated scenario pre-event (upper panel) and post-event (lower panel). In the pre-event scenario, the scattering is dominated by the presence of the vegetation whereas geometric factors play an important role in the post-event scenario.

or symmetry according to the considered techniques. On the other hand, the coherence analysis shows an increase of such parameters in the post-event image pairs almost corresponding to the stripe of increased values of the other techniques. Moreover, it also allows the detection of some effects of the phenomenon mainly due to the presence of mud, in the lower part of Mt. Epomeo, closer to the Casamicciola urban area. Such behaviors can be explained by taking into account both the geometry of view of the CSG SAR sensor according to the topography of the area and the signal scattering properties depending on the features of the investigated scenario.

The presence of large vegetated areas before the event returns in a mechanism of backscattering known as volume scattering [33] characterized by quite higher values than the scattering due to a rough surface such as the soil composed of mud, water, and debris after the event. Moreover, the landslide-mudflow activated along a channel where the topography shows an incision of several meters previously formed likely due to water erosive effects. Then, after the event which destroyed the vegetation, such morphology should produce geometric distortions typical of SAR images known as shadowing, layover, and foreshortening [34], because of the incidence angle of about 27° and the geometry of view observing from the east to west along the descending track of the CSG SAR sensor. In particular, by observing Fig. 11, it is clear how the eastern section of the channel undergoes a shadowing effect with typically low values of backscattered intensity and symmetry. Instead, the eastern section is mainly affected by foreshortening and layover effects which produce a bright stripe due to the sum of several contributions in the same backscattered pulse with consequent high values of intensity and symmetry in the post-event image. Then, the combination of the lack of vegetation and the SAR geometric distortions produces the pattern detected by Δi_{HH}, Δi_{HV}, λ, and Δr techniques with two stripes of increased and decreased values.

In a similar way, the increased values of coherence along the western side of the channel are strictly connected to the vegetation. Large vegetated areas such as the one before the event are typically subjected to temporal decorrelation effects which strongly affect the SAR signal causing coherence loss. Conversely, in the post-event image, the coherence increases since the vegetation was completely destroyed in the channel by the landslide-mudflow and the soil does not change its electromagnetic response to the SAR signal. The same effect is observed in the lower part of the phenomenon however the scenario is quite different since that area was characterized by some agricultural fields and residential houses with gardens before the event which still cause coherence loss and a large presence of mud post-event which was able to agglomerate due to the lower slope and produce a coherence increase.

Finally, the coherence increase shown in the surrounding is likely due to the different perpendicular baseline characterizing the two pairs, which is about 250 m and 57 m for the pre- and post-event pair, respectively.

VII. Conclusion

In this work, several data processing techniques were applied to a dataset of SAR images acquired by CSG missions to detect the landslide-mudflow event that hit Ischia island on November 26th. The aim has been to fully explore the capabilities of both the amplitude and the phase of the SAR signal to map any changes on the ground induced by the event. Both SP and DP configurations have been exploited returning five detection methods with several features. Experimental results show how all the techniques are able to detect the main landslide event with the best performance highlighted by the one based on the reflection symmetry property. On the other hand, accumulations of mud in areas characterized by a low slope are better constrained by the one based on coherence variation. This study demonstrates how, depending on the geometry of the view of satellites and the features of the investigated scenario, a detection method can work better than the others. Then, in such complex cases, it is advisable to use all the techniques to have a synoptic view of the ongoing phenomenon as much reliably as possible. This study also demonstrates how useful can be satellite data for emergency support in case of natural disasters. The time window ideally indicated to provide useful information for the management of postcrisis scenarios, such as the mapping of

the areas affected by landslide phenomena, is within 2 weeks from the event [35]. However, in some cases, satellite revisit time in the order of 15–16 days could not be appropriate, especially considering *X*-band data and complex scenarios as mountainous areas strongly affected by tropospheric artifacts and decorrelation effects due to vegetation or snow.

In this sense, it is important to remark the importance of the availability of increased satellite data both for the present and future space missions at least for those areas potentially affected by natural hazards such as Ischia island.

Acknowledgment

The authors would like to thank the Italian Space Agency for providing the data. Project carried out using COSMO-SkyMed Products, © of the Italian Space Agency (ASI), delivered under a license to use by ASI.

References

[1] L. D'Auria et al., "The seismicity of Ischia island," *Seismol. Res. Lett.*, vol. 89, no. 5, pp. 1750–1760, 2018, doi: 10.1785/0220180084.

[2] A. Tramelli et al., "The seismic network of Ischia island from 1993 to 2021," *Geol. Soc. Special Pub.*, vol. 519, pp. SP519–S2021, 2022, doi: 10.1144/SP519-2021-192.

[3] A. Galvani, G. Pezzo, V. Sepe, and G. Ventura, "Shrinking of Ischia island (Italy) from long-term geodetic data: Implications for the deflation mechanisms of resurgent calderas and their relationships with seismicity," *Remote Sens.*, vol. 13, no. 22, 2021, Art. no. 4648, doi: 10.3390/rs13224648.

[4] L. Beccaro et al., "Multitemporal and multisensor InSAR analysis for ground displacement field assessment at Ischia volcanic island (Italy)," *Remote Sens.*, vol. 13, no. 21, 2021, Art. no. 4253, doi: 10.3390/rs13214253.

[5] M. Albano et al., "The relationship between InSAR coseismic deformation and earthquake-induced landslides associated with the 2017 Mw 3.9 Ischia (Italy) earthquake," *Geosciences*, vol. 8, no. 8, Aug. 2018, Art. no. 303, doi: 10.3390/geosciences8080303.

[6] V. D. Novellis et al., "The 21 August 2017 Ischia (Italy) earthquake source model inferred from seismological, GPS, and DInSAR measurements," *Geophys. Res. Lett.*, vol. 45, pp. 2193–2202, 2018, doi: 10.1002/2017GL076336.

[7] R. Nappi et al., "The 21 August 2017 Md 4.0 casamicciola earthquake: First evidence of coseismic normal surface faulting at the Ischia volcanic island," *Seismol. Res. Lett.*, vol. 89, no. 4, pp. 1323–1334, 2018, doi: 10.1785/0220180063.

[8] J. S. Kargel et al., "Geomorphic and geologic controls of geohazards induced by Nepal's 2015 Gorkha earthquake," *Science*, vol. 351, no. 6269, 2016, Art. no. aac8353, doi: 10.1126/science.aac8353.

[9] T. R. Robinson, N. Rosser, and R. J. Walters, "The spatial and temporal influence of cloud cover on satellite-based emergency mapping of earthquake disasters," *Sci. Rep.*, vol. 9, no. 1, 2019, Art. no. 12455, doi: 10.1038/s41598-019-49008-0.

[10] K. Burrows, R. J. Walters, D. Milledge, and A. L. Densmore, "A systematic exploration of satellite radar coherence methods for rapid landslide detection," *Natural Hazards Earth Syst. Sci.*, vol. 20, no. 11, pp. 3197–3214, 2020, doi: 10.5194/nhess-20-3197-2020.

[11] T. Konishi and Y. Suga, "Landslide detection using COSMO-SkyMed images: A case study of a landslide event on Kii Peninsula, Japan," *Eur. J. Remote Sens.*, vol. 51, no. 1, pp. 205–221, 2018, doi: 10.1080/22797254.2017.1418185.

[12] R. Nappi, G. Alessio, and E. B. Sessa, "A case study comparing landscape metrics to geologic and seismic data from the Ischia island (Southern Italy)," *Appl. Geomatics*, vol. 2, pp. 73–82, 2010, doi: 10.1007/s12518-010-0023-z.

[13] V. Acocella and R. Funiciello, "The interaction between regional and local tectonics during resurgent doming: The case of the island of Ischia, Italy," *J. Volcanol. Geothermal Res.*, vol. 88, pp. 109–123, 1999, doi: 10.1016/S0377-0273(98)00109-7.

[14] L. Vezzoli, *Island of Ischia*. Rome, Italy: CNR, Quaderni De La Ricerca Scientifica, 1988.

[15] G. Orsi, G. Gallo, and A. Zanchi, "Simple-shearing block resurgence in caldera depressions. A model from Pantelleria and Ischia," *J. Volcanol. Geothermal Res.*, vol. 47, pp. 1–11, 1991, doi: 10.1016/0377-0273(91)90097-J.

[16] R. Nappi et al., "The 2017, MD = 4.0, Casamicciola earthquake: ESI-07 scale evaluation and implications for the source model," *Geosciences*, vol. 11, no. 2, 2021, Art. no. 44, doi: 10.3390/geosciences11020044.

[17] C. D. Gaudio, I. Aquino, C. Ricco, V. Sepe, and C. Serio, "Geodetic surveillance of the Ischia island: Results of the precision levelling performed in June 2010," *Quaderni di Geofisica*, vol. 87, pp. 4–16, 2011.

[18] P. D. Martino, M. Dolce, G. Brandi, G. Scarpato, and U. Tammaro, "The ground deformation history of the Neapolitan volcanic area (Campi Flegrei caldera, Somma–Vesuvius volcano, and Ischia island) from 20 years of continuous GPS observations (2000–2019)," *Remote Sens.*, vol. 13, no. 14, 2021, Art. no. 2725, doi: 10.3390/rs13142725.

[19] G. M. Marmoni, S. Martino, M. J. Heap, and T. Reuschlé, "Gravitational slope-deformation of a resurgent caldera: New insights from the mechanical behaviour of Mt. Nuovo tuffs (Ischia island, Italy)," *J. Volcanol. Geothermal Res.*, vol. 345, pp. 1–20, 2017, doi: 10.1016/j.jvolgeores.2017.07.019.

[20] J. Selva et al., "Multiple natural hazards at volcanic islands: A review for the Ischia volcano (Italy)," *J. Appl. Volcanol.*, vol. 8, no. 5, 2019, Art. no. 5, doi: 10.1186/s13617-019-0086-4.

[21] J. S. Lee, L. Jurkevich, P. Dewaele, P. Wambacq, and A. Oosterlinck, "Speckle filtering of synthetic aperture radar images: A review," *Remote Sens. Rev.*, vol. 8, no. 4, pp. 313–340, 1994, doi: 10.1080/02757259409532206.

[22] R. Touzi, "A review of speckle filtering in the context of estimation theory," *IEEE Trans. Geosci. Remote Sens.*, vol. 40, no. 11, pp. 2392–2404, Nov. 2002, doi: 10.1109/TGRS.2002.803727.

[23] E. J. Fielding et al., "Surface ruptures and building damage of the 2003 Bam, Iran, earthquake mapped by satellite synthetic aperture radar interferometric correlation," *J. Geophys. Res.*, vol. 110, no. B3, 2005, Art. no. B03302, doi: 10.1029/2004JB003299.

[24] S.-H. Yun et al., "Rapid damage mapping for the 2015 Mw 7.8 Gorkha earthquake using synthetic aperture radar data from COSMO–SkyMed and ALOS-2 satellites," *Seismol. Res. Lett.*, vol. 86, no. 6, pp. 1549–1556, 2015, doi: 10.1785/0220150152.

[25] J. Lee and E. Pottier, *Polarimetric Radar Imaging: From Basics to Applications*. New York, NY, USA: Taylor & Francis, 2009, doi: 10.1201/9781420054989.

[26] E. Ferrentino, A. Marino, F. Nunziata, and M. Migliaccio, "A dual–polarimetric approach to earthquake damage assessment," *Int. J. Remote Sens.*, vol. 40, no. 1, pp. 197–217, 2019, doi: 10.1080/01431161.2018.1511935.

[27] A. Marino and M. Nannini, "Signal models for changes in polarimetric SAR data," *IEEE Trans. Geosci. Remote Sens.*, vol. 60, 2022, Art. no. 5212818, doi: 10.1109/TGRS.2021.3113182.

[28] E. Ferrentino et al., "On the combination of dual-polarization Sentinel-1 ascending/descending orbiting passes to estimate damage due to the 2016 Central Italy earthquake," *IEEE J. Sel. Topics Appl. Earth Observ. Remote Sens.*, vol. 15, pp. 9509–9518, 2022, doi: 10.1109/JSTARS.2022.3217889.

[29] F. Nunziata, M. Migliaccio, and C. E. Brown, "Reflection symmetry for polarimetric observation of man-made metallic targets at sea," *IEEE J. Ocean. Eng.*, vol. 37, no. 3, pp. 384–394, Jul. 2012, doi: 10.1109/JOE.2012.2198931.

[30] E. Ferrentino, F. Nunziata, M. Migliaccio, and A. Vicari, "A sensitivity analysis of dual-polarization features to damage due to the 2016 Central-Italy earthquake," *Int. J. Remote Sens.*, vol. 39, no. 20, pp. 6846–6863, 2018, doi: 10.1080/01431161.2018.1466078.

[31] E. Ferrentino, F. Nunziata, C. Bignami, L. Graziani, A. Maramai, and M. Migliaccio, "Multi-polarization C-band SAR imagery to quantify damage levels due to the Central Italy earthquake," *Int. J. Remote Sens.*, vol. 42, no. 15, pp. 5969–5984, 2021, doi: 10.1080/01431161.2021.1933247.

[32] M. Adil, A. Buono, F. Nunziata, E. Ferrentino, D. Velotto, and M. Migliaccio, "On the effects of the incidence angle on the L-band multi-polarisation scattering of a small ship," *Remote Sens.*, vol. 14, no. 22, 2022, Art. no. 5813, doi: 10.3390/rs14225813.

[33] A. Freeman and S. L. Durden, "A three-component scattering model for polarimetric SAR data," *IEEE Trans. Geosci. Remote Sens.*, vol. 36, no. 3, pp. 963–973, May 1998, doi: 10.1109/36.673687.

[34] T. M. Lillesand, R. W. Kiefer, and J. W. Chipman, *Remote Sensing and Image Interpretation*. Hoboken, NJ, USA: Wiley, 2015.

[35] "Multi-sector initial rapid assessment guidance - Revision July 2015," *Humanitarian Response*, 2015. [Online]. Available: https://www.humanitarianresponse.info/en/programme-cycle/space/document/multi-sector-initial-rapid-assessment-guidance-revision-july-2015

Marco Polcari was born in Naples, Italy, on October 17, 1984. He received the M.Sc. degree in telecommunication engineering from the University Naples Federico II, Naples, Italy, in 2012, and the Ph.D. degree in geophysics from the University of Bologna, Bologna, Italy, in 2016 .

Since 2012, he has been a researcher with the Istituto Nazionale di Geofisica e Vulcanologia, Rome, Italy. He is involved in Italian and international projects and is the author of several peer-reviewed articles and conference papers. His main research interests include multitemporal synthetic aperture radar (SAR) interferometry data processing and analysis for surface deformation induced by natural phenomena and SAR and GPS data fusion for retrieving a 3-D knowledge of a displacement field. In particular, his skills are in seismic, volcanic, and urban areas evaluating the displacement field due to a coseismic event, slow displacements characterizing the interseismic phase of an earthquake, volcanoes inflation/deflation, landslides, and urban subsidence.

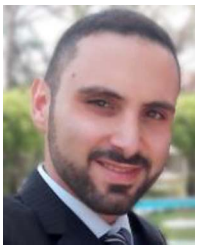

Emanuele Ferrentino (Graduate Student Member, IEEE) was born in Cattolica, Italy, in 1984. He received the B.Sc. and M.Sc. degrees in telecommunication engineering from the Università di Napoli "Parthenope," Naples, Italy, in 2010 and 2014, respectively, and the Ph.D. degree in information engineering from the Università degli Studi di Napoli "Parthenope," Naples, Italy, in 2019.

He is currently a Postdoc Researcher with the Istituto Nazionale di Geofisica e Vulcanologia, Rome, Italy. His research interests include electromagnetic modeling, polarimetric synthetic aperture radar data analysis, and remote sensing land and marine applications (earthquake damage assessment, lava flow detection, change detection, target detection, coastline extraction, and classification).

Christian Bignami (Member, IEEE) received the M.S. degree in telecommunication engineering and the Ph.D. degree in electromagnetism from the Sapienza University of Rome, Rome, Italy, in 2002 and 2008, respectively.

Since 2007, he has been a Researcher with the Istituto Nazionale di Geofisica e Vulcanolgia, Rome, Italy, and a member of the Remote Sensing Unit, Rome, Italy. He is involved in several national and international research projects based on EO data exploitation and monitoring. His main research interests include synthetic aperture radar and optical satellite data processing and analysis for surface deformation and change detection, EO, and ground data integration.

Sven Borgstrom received the M.S. degree in geological sciences and the Ph.D. degree in geophysics from the University of Naples Federico II, Naples, Italy, in 1983 and 1990, respectively.

He was with the University of Naples Federico II. Since 2003, he has been a Technical Researcher with the Istituto Nazionale di Geofisica e Vulcanologia, the Naples branch. He is responsible for research projects and monitoring activities with the Italian Civil Protection Department. His main research interests include the interferometric synthetic aperture radar (InSAR) space-borne data processing for ground deformation studies in active volcanic areas, besides the InSAR analysis for coseismic/postseismic deformation measurements in seismogenic areas worldwide. He also works on the integration of InSAR results with ground-based geodetic data (mainly cGNSS) for monitoring and research activities.

Rosa Nappi received the M.S. degree in geological sciences from the Department of Geological Sciences, University Naples Federico II, Naples, Italy, in 1995, and qualified to practice as a Geologist, in 1996.

From 1998 to 2003, she was with the Istituto Nazionale di Geofisica. Since 2003, she has been a Technologist with the Istituto Nazionale di Geofisica e Vulcanologia, Osservatorio Vesuviano, Naples, Italy. Her main research interests include the study of active faults in tectonic and volcanic areas and the study of the primary and secondary effects produced on the ground by an earthquake and/or by natural events with the aim of contributing to the knowledge of seismic and environmental hazards. In particular, she studies the ground deformations through geomorphic-quantitative analysis from high-resolution DTMs, Lidar data, aerial photogrammetric analysis, and field surveys, in a GIS environment, integrated with the analysis of geophysical and macroseismic data. The areas which she recently studied are as follows: Ischia island (August 21, 2017, Casamicciola earthquake and Ischia landslide 2022); Central Apennines (Eagle earthquake and Amatrice-Visso-Norcia seismic sequences 2016/17) Salento Peninsula (Puglia Region, Southern Italy); and Campania Plain. She is currently involved in various national and international research projects (INQUA project, METIQ project, INGV Ricerca Libera, and FAC project) and has collaborated with the University of Naples Federico II, University of Insubria, Como and CNR-ISA, Avellino, Naples.

Valeria Siniscalchi was born in Polla, Salerno, Italy, on May 14, 1961. She received the M.S. degree in geological sciences from the Department of Geological Sciences, Siena University, Siena, Italy, in 1987.

Since 1996, she has been a Technologist with Istituto Nazionale di Geofisica e Vulcanologica, Osservatorio Vesuviano, Naples, Italy. Her research interests include the study of ground deformations of the Neapolitan Volcanic District and also of areas outside of it, by synthetic aperture radar data in the different wavelengths of acquisition. She collaborates with universities and research centers. She is the author of papers published in national and international journals, surveillance reports, and abstracts concerning ground deformation study by satellite data and integrated geodetic methodology (GPS data, high-precision leveling, tilt-metric data) of volcanic and tectonic areas of Italy and other volcanic areas in the world. She is involved in Italian and international projects and has been the Point of Contact for the subtask WP5.15 (All.A Department of Civil Protection) "Satellite Monitoring-Ischia Island" since 2018. She also carries out dissemination and communication activities. She participates in GPS and leveling measurements surveys in Neapolitan Volcanic District, Aeolian Island, and surface coseismic fracture field surveys with SEG (Geological Emergency Services). Since 1999, she has been carrying out Seismic Surveillance h24 at the Monitoring Center of INGV-Osservatorio Vesuviano.